

Electronic Supporting Information

Reduction of Graphite Oxide Using Alcohols

Daniel R. Dreyer^a, Shanthi Murali^b, Yanwu Zhu^b, Rodney S. Ruoff^b, and Christopher W. Bielawski *^a

^a Department of Chemistry and Biochemistry, The University of Texas at Austin, 1 University Station, A5300, Austin, TX, 78712, USA

^b Department of Mechanical Engineering and the Texas Materials Institute, The University of Texas at Austin, 1 University Station, C2200, Austin, TX, 78712, USA..

E-mail: bielawski@cm.utexas.edu

Synthetic Details	S3–S4
General Considerations	S3
Synthetic Procedures	S3–S4
Elemental Analyses	S5
Table S1. Combustion analysis data for GO and reduced carbons.	S5
Surface Analysis	S6–S10
Figure S1. BET plot for GO.	S6
Figure S2. BET plot for MeOH-reduced GO.	S7
Figure S3. BET plot for EtOH-reduced GO.	S8
Figure S4. BET plot for iPrOH-reduced GO.	S9
Figure S5. BET plot for BnOH-reduced GO.	S10
Table S2. Summary of BET data.	S10
Bulk Powder Conductivity Measurements	S11–S16
Figure S6. Conductivity plot for GO.	S12
Figure S7. Conductivity plot for MeOH-reduced GO.	S13
Figure S8. Conductivity plot for EtOH-reduced GO.	S14
Figure S9. Conductivity plot for iPrOH-reduced GO.	S15
Figure S10. Conductivity plot for BnOH-reduced GO.	S16
Table S3. Summary of bulk powder conductivity data.	S16
Reduction of GO Using Other (Non-alcoholic) Substrates	S17
Table S4. Summary of elemental analysis and powder conductivity data.	S17
Powder XRD Analyses	S18–S19

Figure S11. Spectra of GO and reduced carbons.	S18
Table S5. Summary of XRD data.	S19
SEM Analyses	S20–S22
Figure S12. SEM image of BnOH-reduced GO.	S20
Figure S13. SEM image of BnOH-reduced GO.	S21
Figure S14. SEM image of BnOH-reduced GO.	S22
TEM Analyses	S23–S27
Figure S15. Diffraction pattern	S23
Figure S16. High resolution TEM image of BnOH-reduced GO.	S24
Figure S17. High resolution TEM image of BnOH-reduced GO.	S25
Figure S18. High resolution TEM image of BnOH-reduced GO.	S26
Figure S19. High resolution TEM image of BnOH-reduced GO.	S27
Ultracapacitor Characterization	S28–S30
Figure S20. Schematic of two-electrode test cell assembly	S28
Figure S21. Galvanostatic charge-discharge plot of BnOH-reduced GO.	S29
Figure S22. Nyquist plot of BnOH-reduced GO.	S30
References	S31

General Considerations. All chemical reagents were purchased from commercial sources and used without additional purification. Unless otherwise noted, all experiments were performed under ambient conditions. ^1H NMR data were collected on Varian Unity INOVA 400 MHz and Varian Mercury 300 MHz spectrometers. Chemical shifts (δ) are referenced downfield from $(\text{CH}_3)_4\text{Si}$ using the residual solvent peak as an internal standard (CDCl_3 , 7.24 ppm for ^1H). TEM data were collected on a JEOL 2010F field emission transmission electron microscopy at 200 kV. XRD data were collected on a Philips X'Pert PRO multipurpose X-ray diffractometer with an incident wavelength of 1.54 Å. Micro-Raman spectra were recorded on a WiTec Alpha300 system with an incident wavelength of 532 nm. SEM data were collected on a Zeiss Supra 40 VP scanning electron microscope. Elemental analyses were performed by Midwest Microlabs, LLC (Indianapolis, IN). BET surface area measurements were performed by nitrogen adsorption on a Quantachrome NOVA 2000 surface analyzer. FT-IR spectra (KBr) were recorded using a Perkin-Elmer Spectrum BX spectrometer. Ultracapacitor characterization was performed using a CH Instruments 660D or an Autolab PGSTAT128N potentiostat.

Preparation of graphite oxide (GO) using the Hummers method.¹ A 100 mL reaction flask was charged with natural flake graphite (2.04 g; SP-1, Bay Carbon Inc. or Alfa Aesar [99%; 7-10 µm]), concentrated sulfuric acid (50 mL), and a stir bar, and then cooled on an ice bath. The flask was then slowly charged with KMnO_4 (6.13 g) over 2 h which afforded a dark colored mixture. After stirring at 0 °C for 1 h, the mixture was stirred for an additional 2 h at room temperature and then at 35 °C for 3 h. The flask was then cooled to room temperature and the resulting viscous dispersion was poured into 1 L of deionized water. A 30% aqueous solution of H_2O_2 (5 mL) was then added slowly to the aqueous mixture, concomitant with gas evolution. The resulting vibrant yellow mixture was then filtered through a coarse fritted funnel or a nylon membrane filter (0.2 µm, Whatman), and the isolated material was washed with additional 6 N HCl (1 L) and deionized water (2 L). The filtered solids were collected and dried under high vacuum to afford the desired product (4.16 g) as a dark brown powder, which was further characterized by elemental combustion, FT-IR, BET surface area, and powder conductivity analyses (see below).

General Reduction Method Using Alcohols. A 50 mL reaction flask was charged with GO (200 mg; prepared via the Hummers method, as described above) and 25 mL of methanol (MeOH), ethanol (EtOH), isopropanol (iPrOH), or benzyl alcohol (BnOH). A Liebig condenser was then attached to the neck and the mixture was heated at 100 °C (BnOH) or reflux (MeOH, EtOH, or iPrOH) for 5 days. The mixture was then poured into 500 mL of EtOH to facilitate precipitation of the dispersion. The agglomerated, black powder was then collected by vacuum filtration and dried under vacuum. Recovered masses were as follows: MeOH: 184.3 mg; EtOH: 162.1 mg; iPrOH: 118.5 mg; BnOH: 111.7 mg.

Elemental Analyses. Elemental combustion analyses were performed in duplicate (see Table S1) on GO samples prepared via the Hummers method, as well as GO reduced by MeOH, EtOH, iPrOH, and BnOH using the method described above.

Table S1. Summary of combustion analysis data (n. f. = none found; - = not tested).

<i>As-Recovered Carbon Product Obtained with the Alcoholic Reductant Noted Below^b</i>					
	Starting GO^a	MeOH	EtOH	iPrOH	BnOH
Carbon	52.35 / 52.29	73.03 / 73.24	80.58 / 80.04	81.57 / 81.64	91.23 / 91.10
Hydrogen	2.05 / 2.06	1.62 / 1.58	1.46 / 1.57	1.94 / 1.98	4.91 / 4.81
Nitrogen	0.15 / 0.14	n. f. / n. f.			
Oxygen	40.94 / 39.95	24.36 / 24.29	17.89 / 18.02	15.99 / 15.84	4.08 / 4.16
Sulfur	3.14 / 3.13	-	-	-	-
Chlorine	1.32 / 1.47	-	-	-	-
TOTAL	99.95 / 99.04	99.01 / 99.11	99.93 / 99.63	99.50 / 99.46	100.22 / 100.07
C:O Ratio	1.70 / 1.75	4.00 / 4.02	6.00 / 5.92	6.80 / 6.87	29.81 / 29.19

^a Prepared via the Hummers method. ^b Prepared by heating 200 mg of GO in 25 mL of the alcohol at 100 °C (MeOH, EtOH, or iPrOH at reflux) for 5 days.

Surface Area Analyses. The surface areas for GO, and the MeOH-, EtOH-, iPrOH-, and BnOH-reduced carbons (200 mg GO in 25 mL alcohol; 5 d at 100 °C [BnOH] or reflux [MeOH, EtOH, iPrOH]) were determined using a 7-point BET method using molecular nitrogen as the adsorbate.² Specific surface areas (in m²·g⁻¹) were determined by converting the isotherms of these measurements into BET plots,² as shown in Figures S1–S5. These surface areas were determined by determining the slope of a line of best fit to Eq. 1 (the BET equation), where W and W_m are the quantities of adsorbed gas and monolayer quantity of adsorbed gas, respectively; P and P_0 are the equilibrium and the saturation pressure of adsorbates; c is the BET constant. The results are summarized in Table S2.

$$\frac{1}{W[(P - P_o) - 1]} = \frac{c - 1}{W_m c} \left(\frac{P}{P_o} \right) + \frac{1}{W_m c} \quad \text{Eq. 1}$$

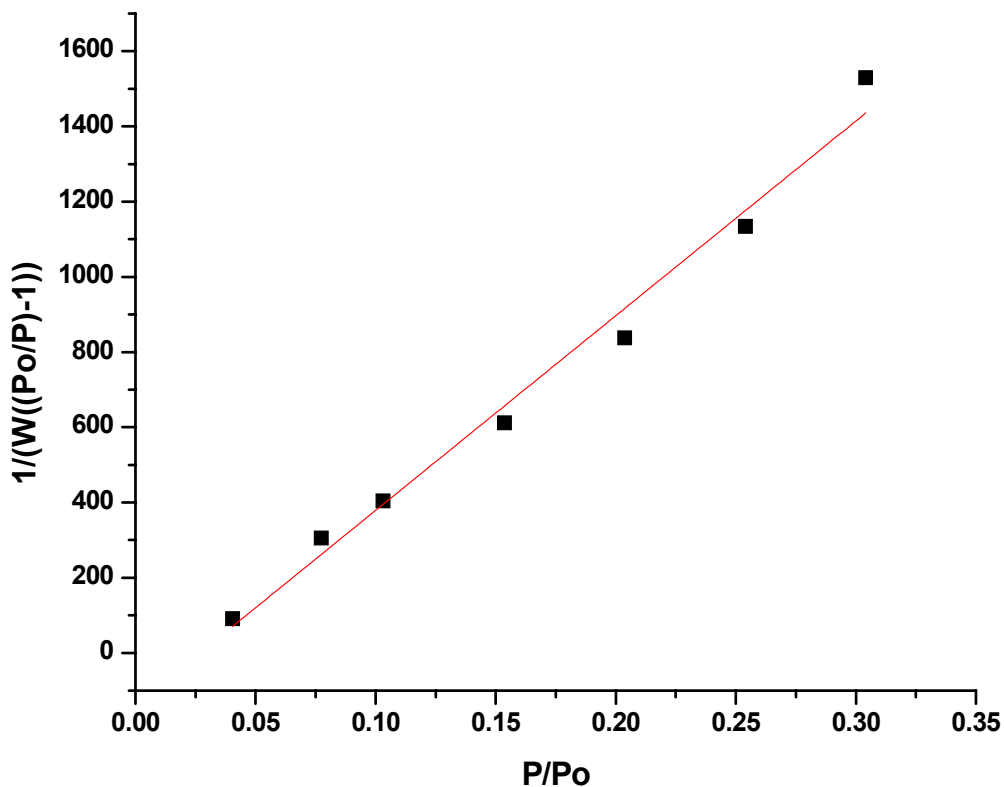


Figure S1. 7-point BET surface area plot of graphite oxide prepared via the Hummers method. W is the quantity of adsorbed gas; P and P_0 are the equilibrium and the saturation pressure of the adsorbate. These results were fit to the BET equation shown in Eq. 1.

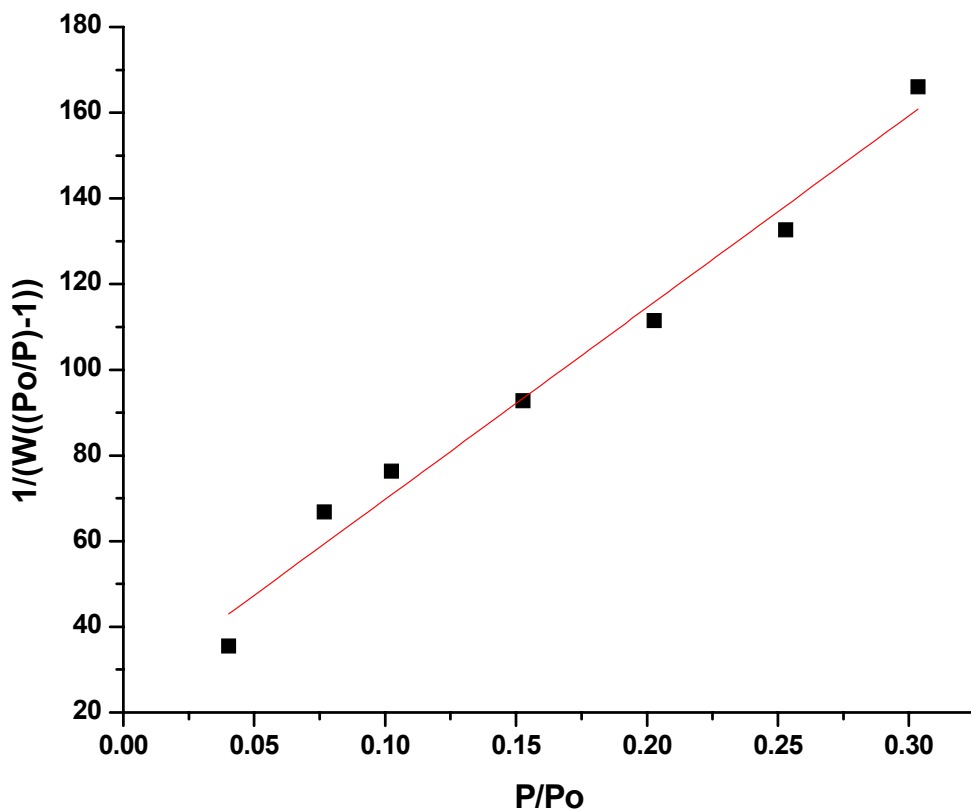


Figure S2. 7-point BET surface area plot of MeOH-reduced GO. W is the quantity of adsorbed gas; P and P_0 are the equilibrium and the saturation pressure of the adsorbate. These results were fit to the BET equation shown in Eq. 1.

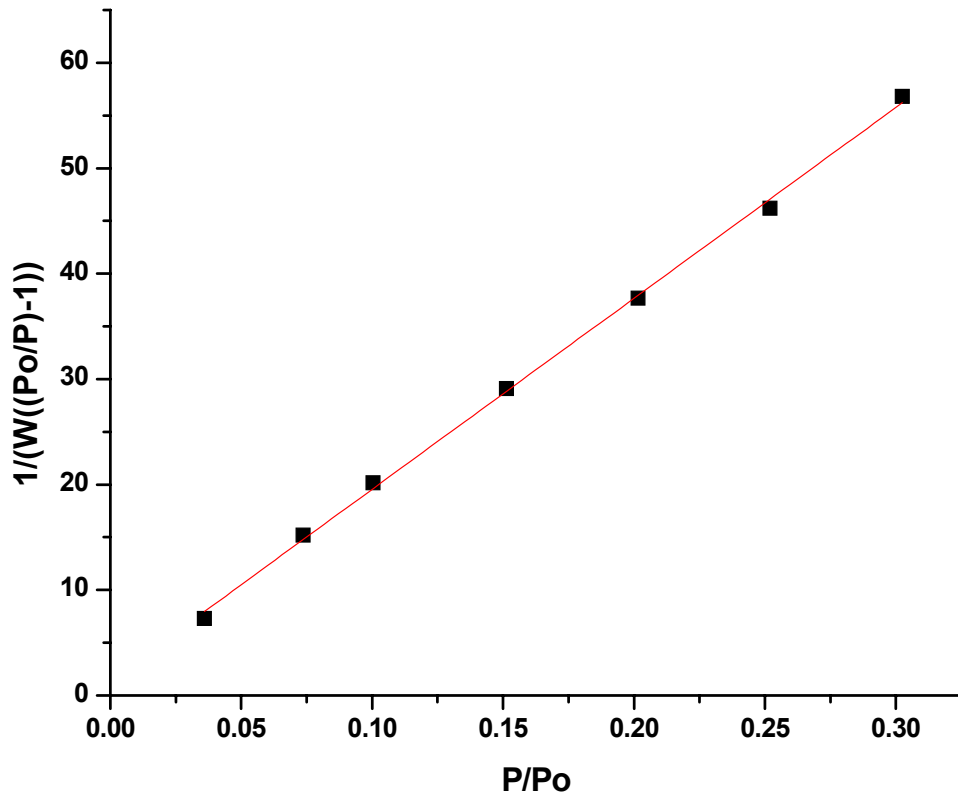


Figure S3. 7-point BET surface area plot of EtOH-reduced GO. W is the quantity of adsorbed gas; P and P_0 are the equilibrium and the saturation pressure of the adsorbate. These results were fit to the BET equation shown in Eq. 1.

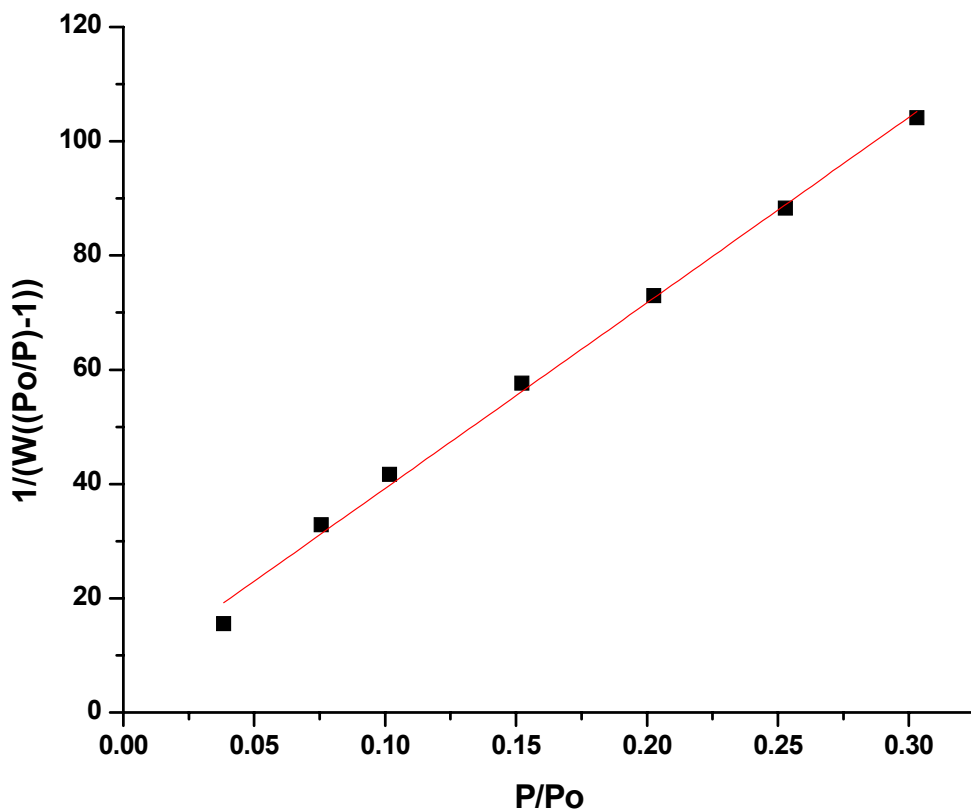


Figure S4. 7-point BET surface area plot of iPrOH-reduced GO. W is the quantity of adsorbed gas; P and P_0 are the equilibrium and the saturation pressure of the adsorbate. These results were fit to the BET equation shown in Eq. 1.

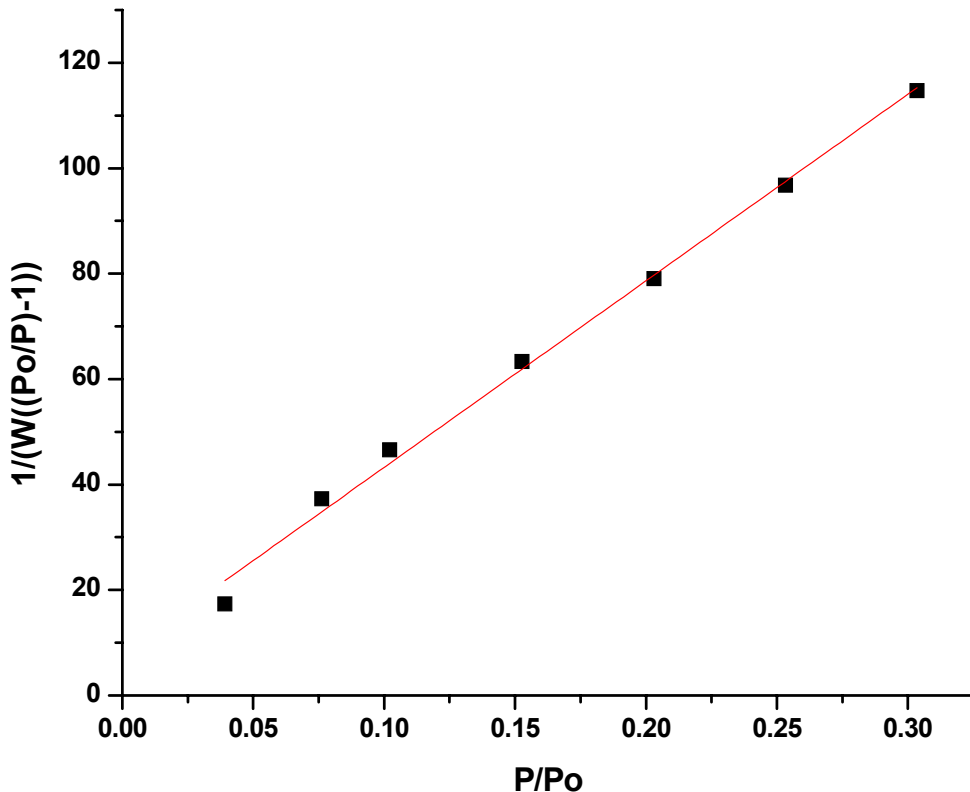


Figure S5. 7-point BET surface area plot of BnOH-reduced GO. W is the quantity of adsorbed gas; P and P_0 are the equilibrium and the saturation pressure of the adsorbate. These results were fit to the BET equation shown in Eq. 1.

Table S2. Summary of BET data.

As-Recovered Carbon Product Obtained with the Reductant Noted Below					
	GO ^a	MeOH ^b	EtOH ^b	iPrOH ^b	BnOH ^b
Area (m²·g⁻¹)	0.6912	7.366	19.08	10.50	9.628
Best Fit Line Slope	5176	447.8	181.0	325.0	353.8
Y-Intercept	-139	24.98	1.455	6.735	7.893
Corr. Coefficient	0.9929	0.9903	0.9994	0.9981	0.9975
BET constant (c)	-36.35	18.93	125.5	49.25	45.83

^a Prepared via the Hummers method. ^b Material recovered after heating 200 mg of GO in 25 mL of the alcohol at 100 °C (BnOH) or at reflux (MeOH, EtOH, or iPrOH at reflux) for 5 days.

Bulk Powder Conductivity Measurements. The electrical conductivity of GO and the MeOH-, EtOH-, iPrOH-, and BnOH-reduced GOs were determined by fitting the observed powder conductivity experimental data (see below) to Eq. 2 with the assumption that the conductivity of the low-conductive phase (air) is zero.³ Briefly, a given quantity of powder (50–100 mg) was poured into a poly(ethylene) tube (ID = 5 mm). The powder was manually compressed between two steel plungers that closely matched the tube's ID. A 5.5 digit Keithley multimeter was connected to the plungers and was used to measure DC resistance by a two-probe method. The plungers were compressed and the resistance was recorded at multiple compression steps (ϕ shown in Eq. 2 below). A digital micrometer was used to measure the height of the powder column at each compression step, allowing for conversion of the measured resistances to conductivities (σ_c in Eq. 2).

$$\sigma_c = \sigma_h \left[\frac{\phi - \phi_c}{1 - \phi_c} \right]^k \quad \text{Eq. 2}$$

where σ_c is the conductivity of the composite medium, σ_h and ϕ are the conductivity of the conductive phase (graphite oxide, or reduced graphite oxide) and their volume fractions respectively, ϕ_c is the percolation threshold, and k is a critical exponent related to the percolation threshold and to the shape of the particles.

The percolation threshold, ϕ_c , is defined as the ratio of the apparent powder density before compression, d_p , and the apparent density of the particles, d_g . The bulk density of graphite (2.2 g cm⁻³) was used³ as a value for d_g . The constants σ_c and ϕ_c were calculated from the parent volume of the reduced GO powders and the resistance of the powders as measured by a multimeter. Figures S6–S10 show σ_c values as a function of ϕ during the compression for GO and the MeOH-, EtOH-, iPrOH-, and BnOH-reduced GO products, respectively. The results are summarized in Table S3.

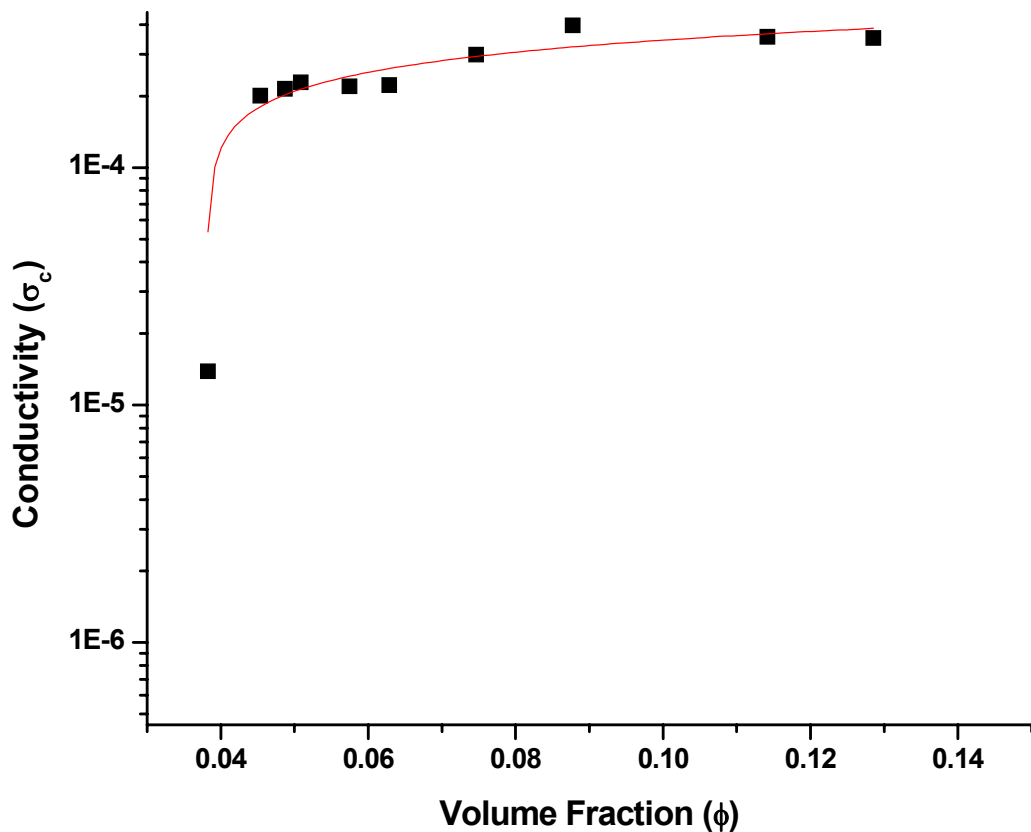


Figure S6. Powder conductivity as a function of compression for graphite oxide (prepared via the Hummers method, as described above). The best fit line using Eq. 1 is shown in red.

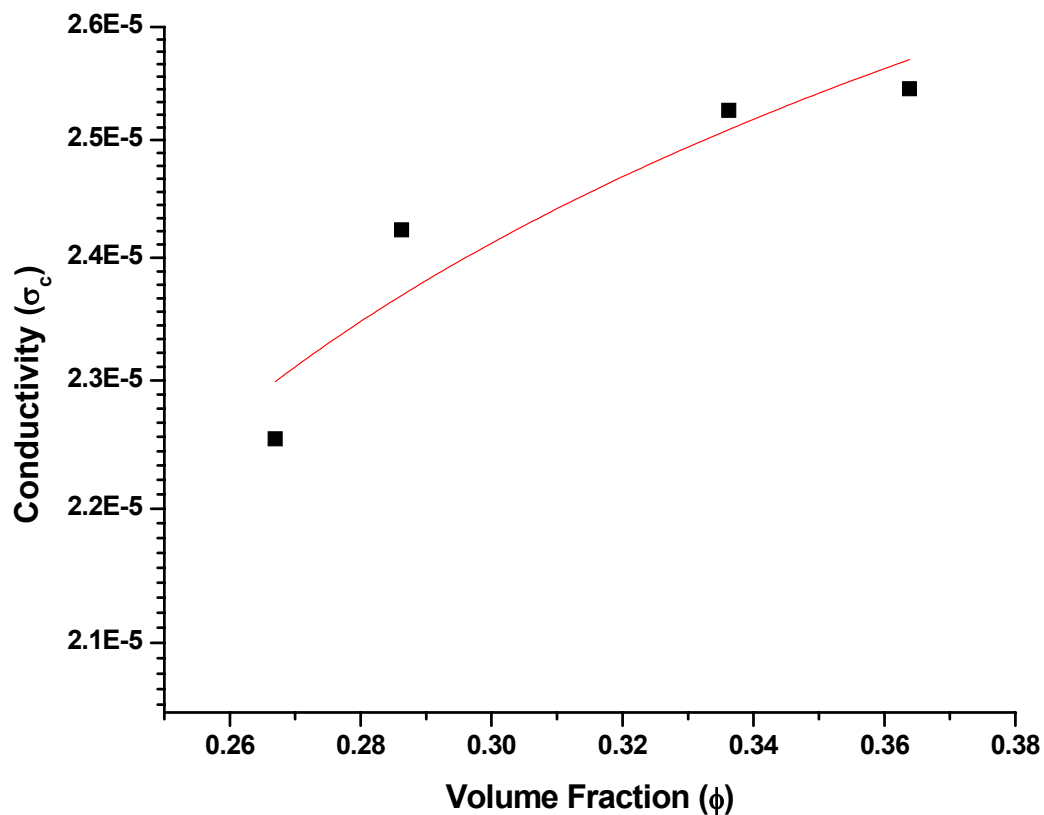


Figure S7. Powder conductivity as a function of compression for MeOH-reduced GO. The best fit line using Eq. 1 is shown in red.

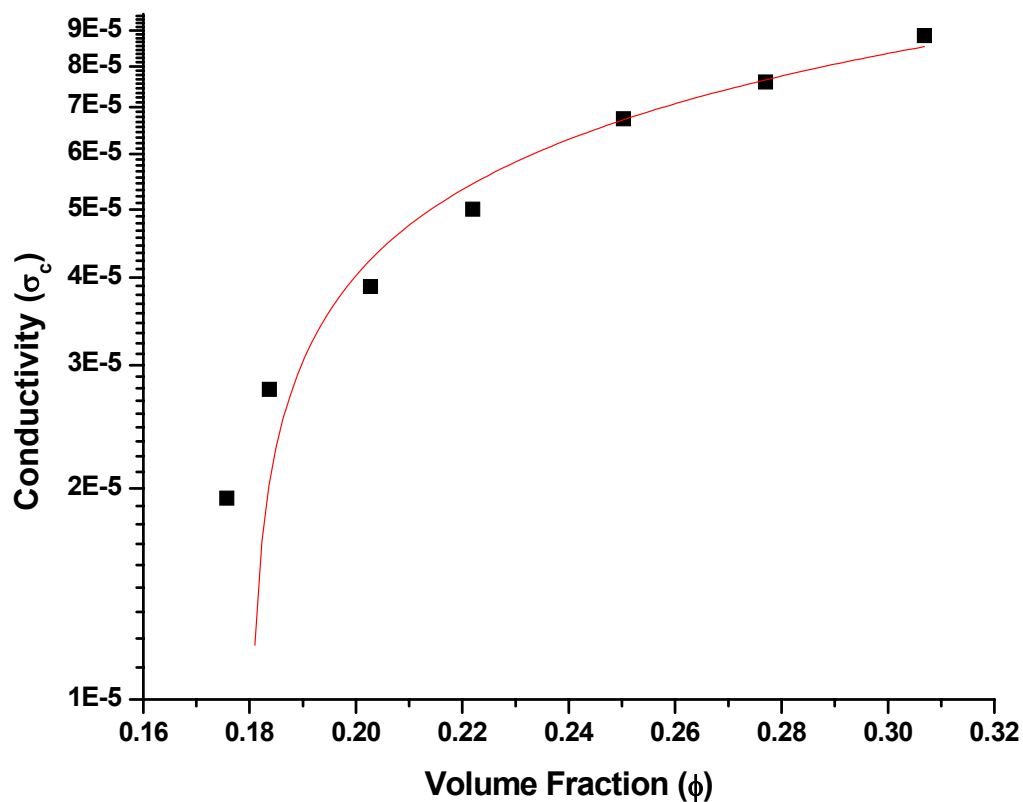


Figure S8. Powder conductivity as a function of compression for EtOH-reduced GO. The best fit line using Eq. 1 is shown in red.

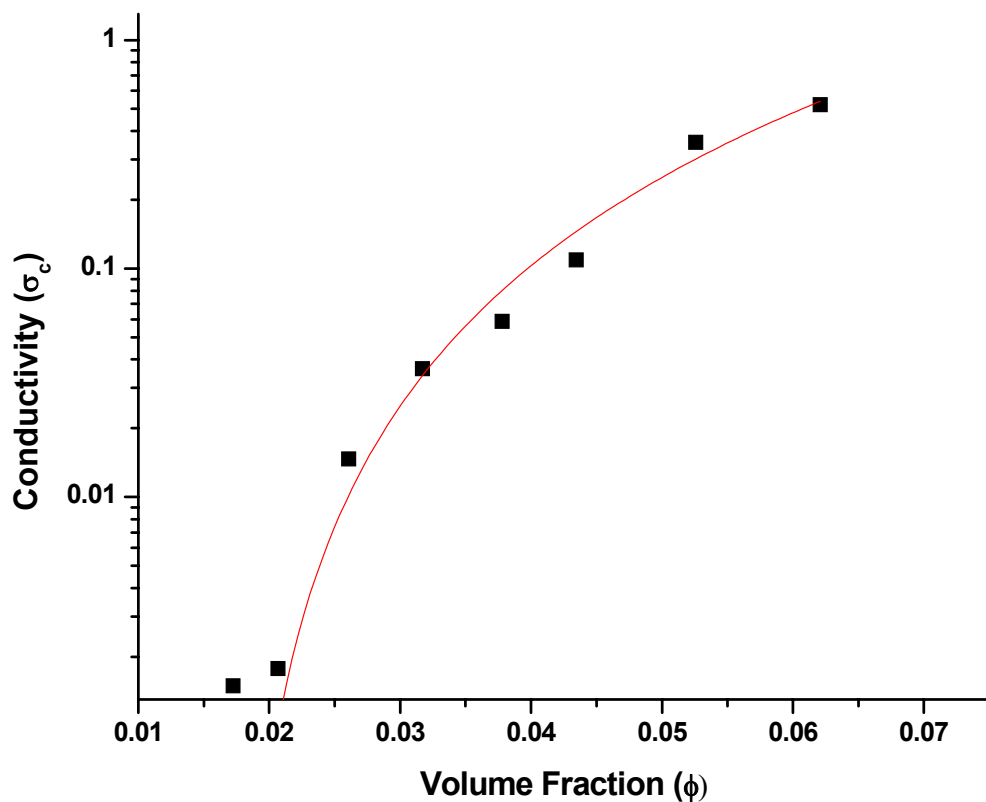


Figure S9. Powder conductivity as a function of compression for iPrOH-reduced GO. The best fit line using Eq. 1 is shown in red.

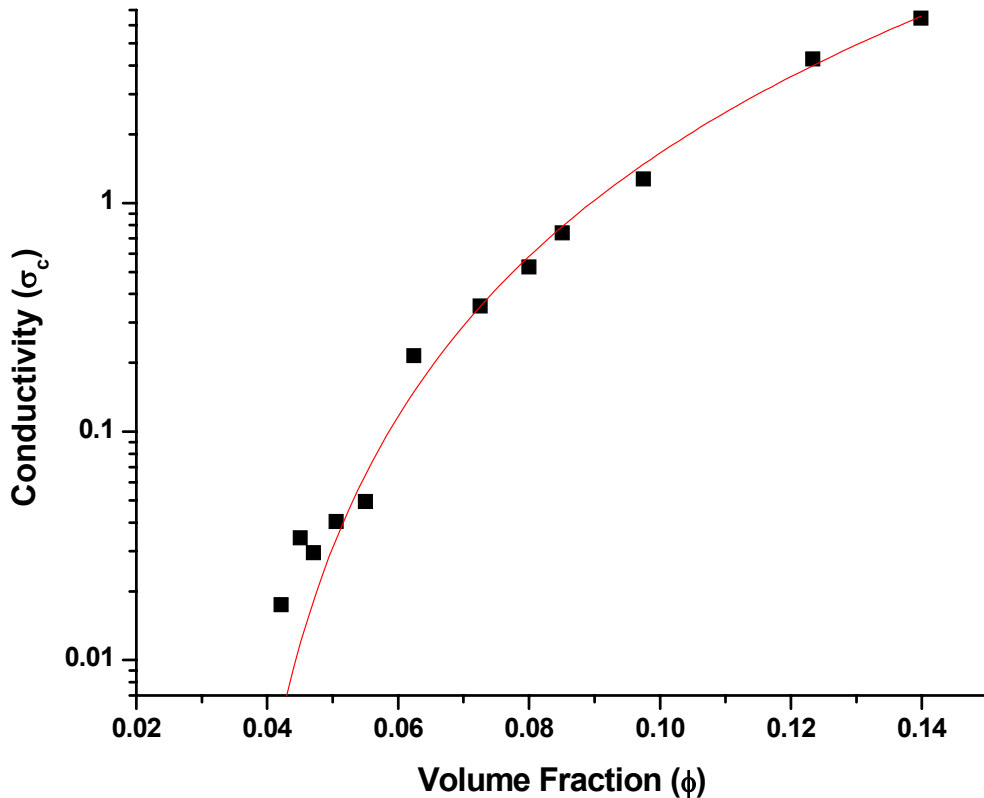


Figure S10. Powder conductivity as a function of compression for BnOH-reduced GO. The best fit line using Eq. 1 is shown in red.

Table S3. Summary of powder conductivity data.

	Powder Conductivity (σ_h ; $S \cdot m^{-1}$) ^a	Critical exponent (k) ^a
GO ^b	7.83×10^{-5}	0.30
MeOH-Reduced GO ^c	3.21×10^{-5}	0.15
EtOH-Reduced GO ^c	1.82×10^{-4}	0.41
iPrOH-Reduced GO ^c	1019.6	2.44
BnOH-Reduced GO ^c	4569.5	2.98

^a Powder conductivity (σ_h) and critical exponent (k) were determined by measuring conductivity (σ_c) as a function of a volume compression (ϕ) and fitting a line of best fit using Eq. 2. ^b Prepared via the Hummers method. ^c Material recovered after heating 200 mg of GO in 25 mL of the alcohol at 100 °C (BnOH) or reflux (MeOH, EtOH, and iPrOH) for 5 days.

Reduction of GO Using Other (Non-alcoholic) Substrates. A series of non-alcoholic, high boiling solvents were used as reduction media under otherwise identical conditions as described in the main text (i.e., 200 mg of GO was heated in 25 mL of solvent for 5 d at 100 °C; the product was precipitated into EtOH and collected by vacuum filtration). The five non-alcoholic solvents shown in Table S4 were selected for their structural and/or chemical similarity (e.g., these solvents' solubility parameters [δ_D , δ_p , δ_H] span benzyl alcohol's parameters) to benzyl alcohol.

Table S4. Summary of solvent solubility parameters, elemental combustion analyses and powder conductivity data for GO reduced by benzyl alcohol, water, propylene carbonate (PC), anisole, and diphenyl ether.^a

Solvent	C : O Ratio ^b	Powder Conductivity (σ_h ; S·m ⁻¹) ^c	Dispersion Solubility Parameter (δ_D) ^d	Polar Solubility Parameter (δ_p) ^d	Hydrogen Bonding Solubility Parameter (δ_H) ^d
Benzyl alcohol	29.9 : 1	4600	18.4	6.3	13.7
Propylene carbonate	4.81	96.8	20.0	18.0	4.1
Water	4.30	149.7	15.5	16.0	42.3
Anisole	3.63	38.4	17.8	4.1	6.7
Benzonitrile	1.88	1.34×10^{-3}	17.4	9.0	3.3
Diphenyl ether	4.58	84.1	19.5	3.4	5.8

^a Material recovered after heating at 100 °C (PC, anisole, dibenzyl ether) or reflux (water) for 5 days. The product was precipitated into EtOH and collected by vacuum filtration. ^b Determined via elemental combustion analysis. ^c Determined using the two-point probe method discussed previously. ^d See Hansen, C. *Hansen Solubility Parameters: A User's Handbook*, 2nd ed.; CRC Press: Hoboken, NJ, 2007.

Powder XRD Analyses. Powder X-ray diffraction analysis plots of GO and reduced GO obtained by reduction with methanol (MeOH), ethanol (EtOH), isopropanol (iPrOH), benzyl alcohol (BnOH), and hydrazine were recorded at a relative humidity of approximately 45% (see Figure S11 and Table S5).

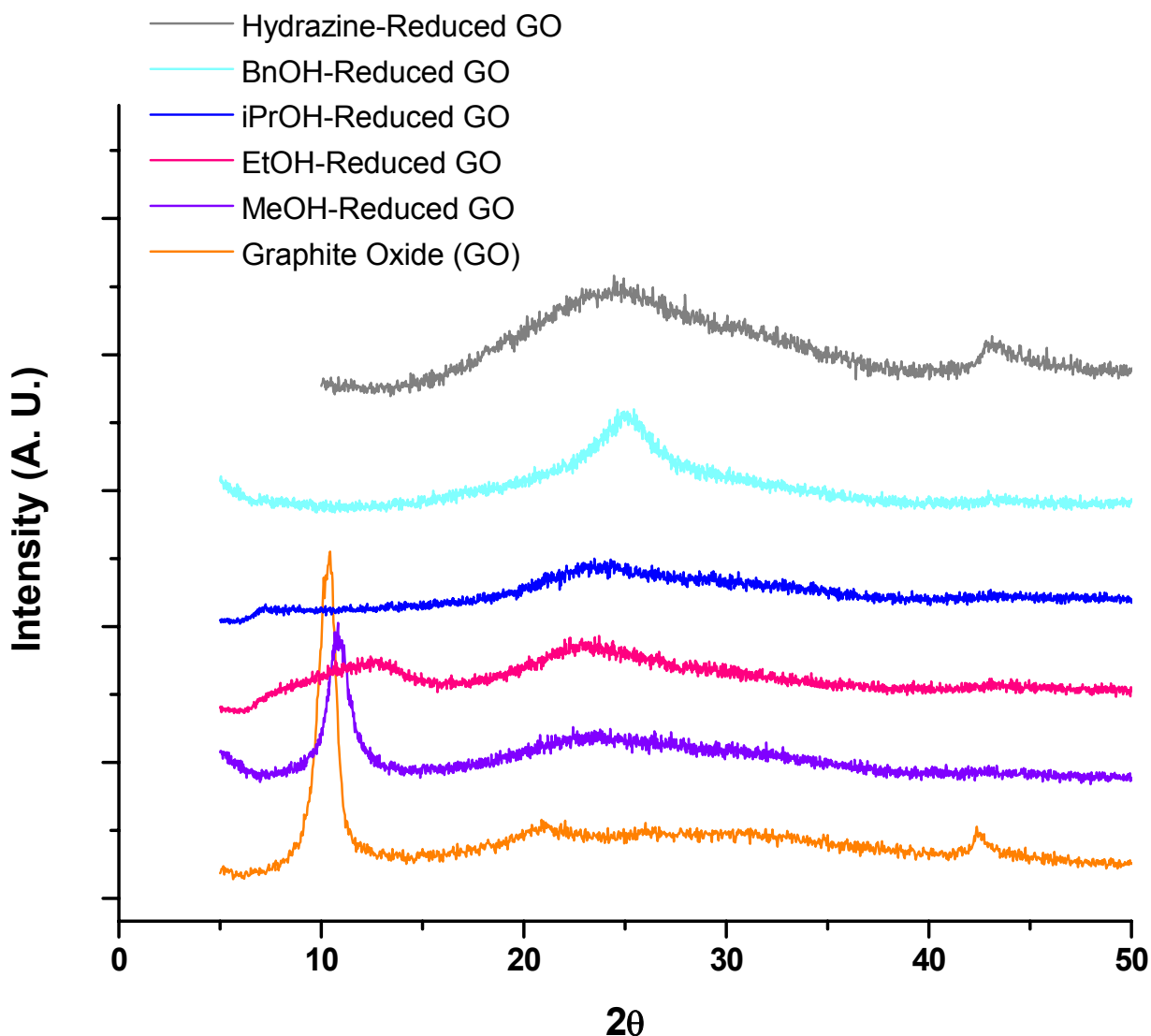


Figure S11. XRD spectra for GO, and MeOH-, EtOH-, iPrOH-, BnOH-, and hydrazine-reduced GO. Measurements were acquired using a source of $\lambda = 1.5405 \text{ \AA}$; temperature = 25 °C; relative humidity = 45%.

Table S5. Summary of XRD data.

Sample	d-spacing (Å)
GO^a	8.47
MeOH-Reduced GO^b	8.11, 3.74
EtOH-Reduced GO^b	7.02, 3.90
iPrOH-Reduced GO^b	3.75
BnOH-Reduced GO^b	3.54
Hydrazine-Reduced GO^c	3.64

^a Prepared via the Hummers method. ^b Material recovered after heating 200 mg of GO in 25 mL of the alcohol at 100 °C (MeOH, EtOH, or iPrOH at reflux) for 5 days. ^c Prepared by dispersing 100 mg of GO in 100 mL of water by sonicating for 3 h, followed by adding 34 µL hydrazine monohydrate and heating at 80 °C for 4 h; product was isolated by vacuum filtration and drying under vacuum.^{3a}

SEM Analyses. Scanning electron microscopy (SEM) images of BnOH-reduced GO were obtained on silica substrates (see Figures S12–S14), and were consistent with the low surface area measured by BET surface analysis and the imagery seen via TEM.

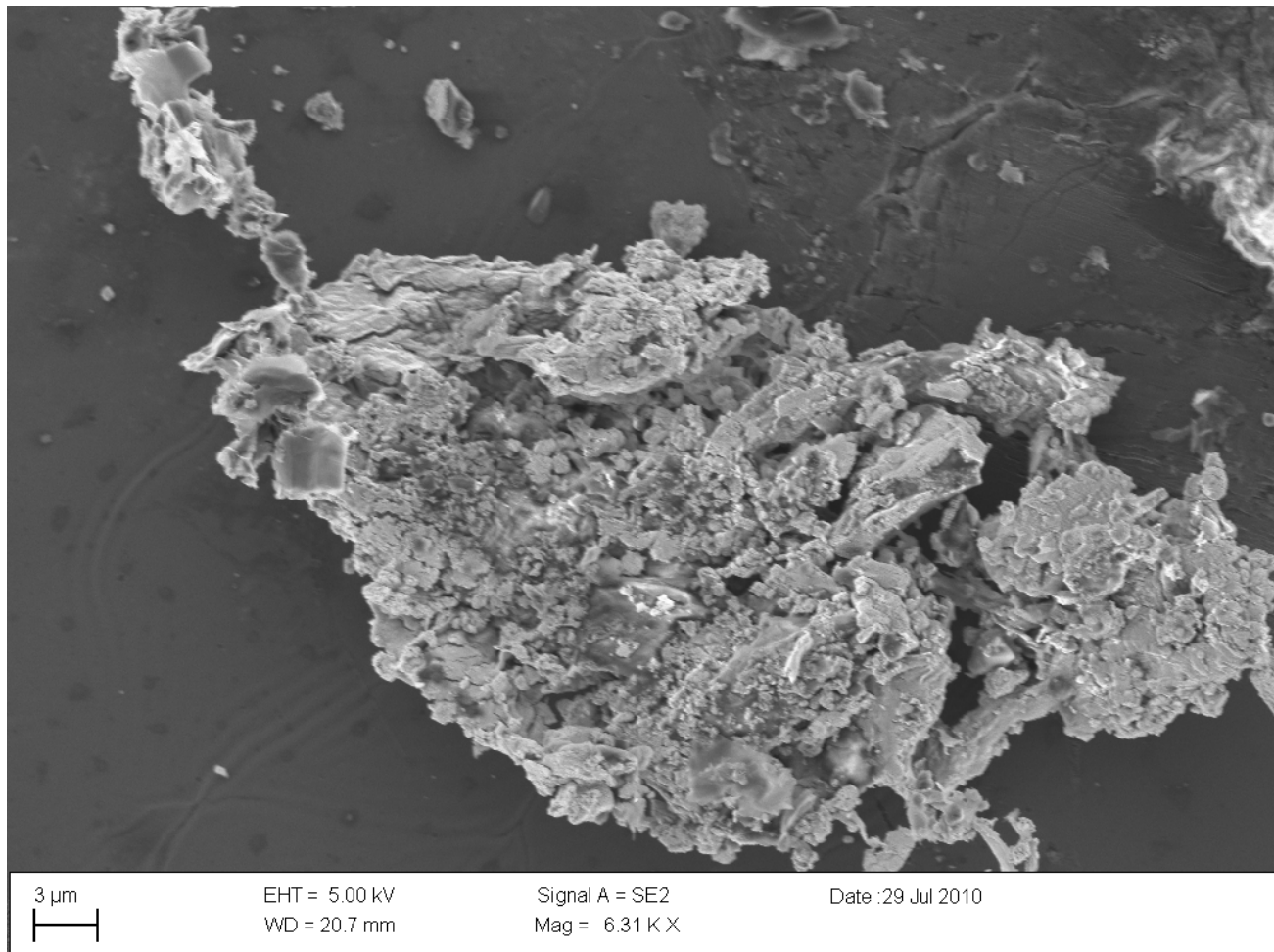


Figure S12. SEM image of as-recovered BnOH-reduced GO showing large, agglomerated particles.

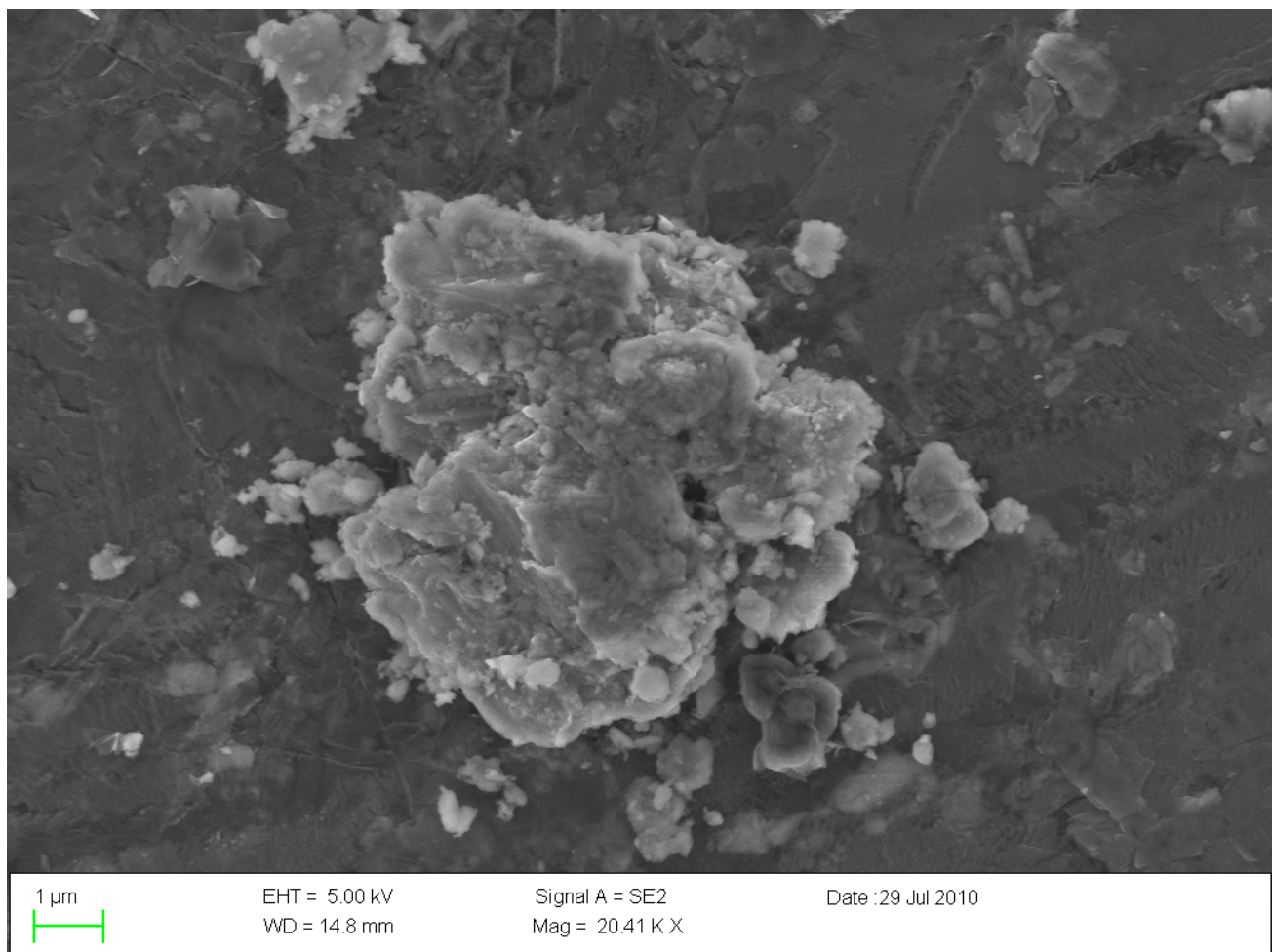


Figure S13. SEM image of as-recovered BnOH-reduced GO showing large, agglomerated particles.

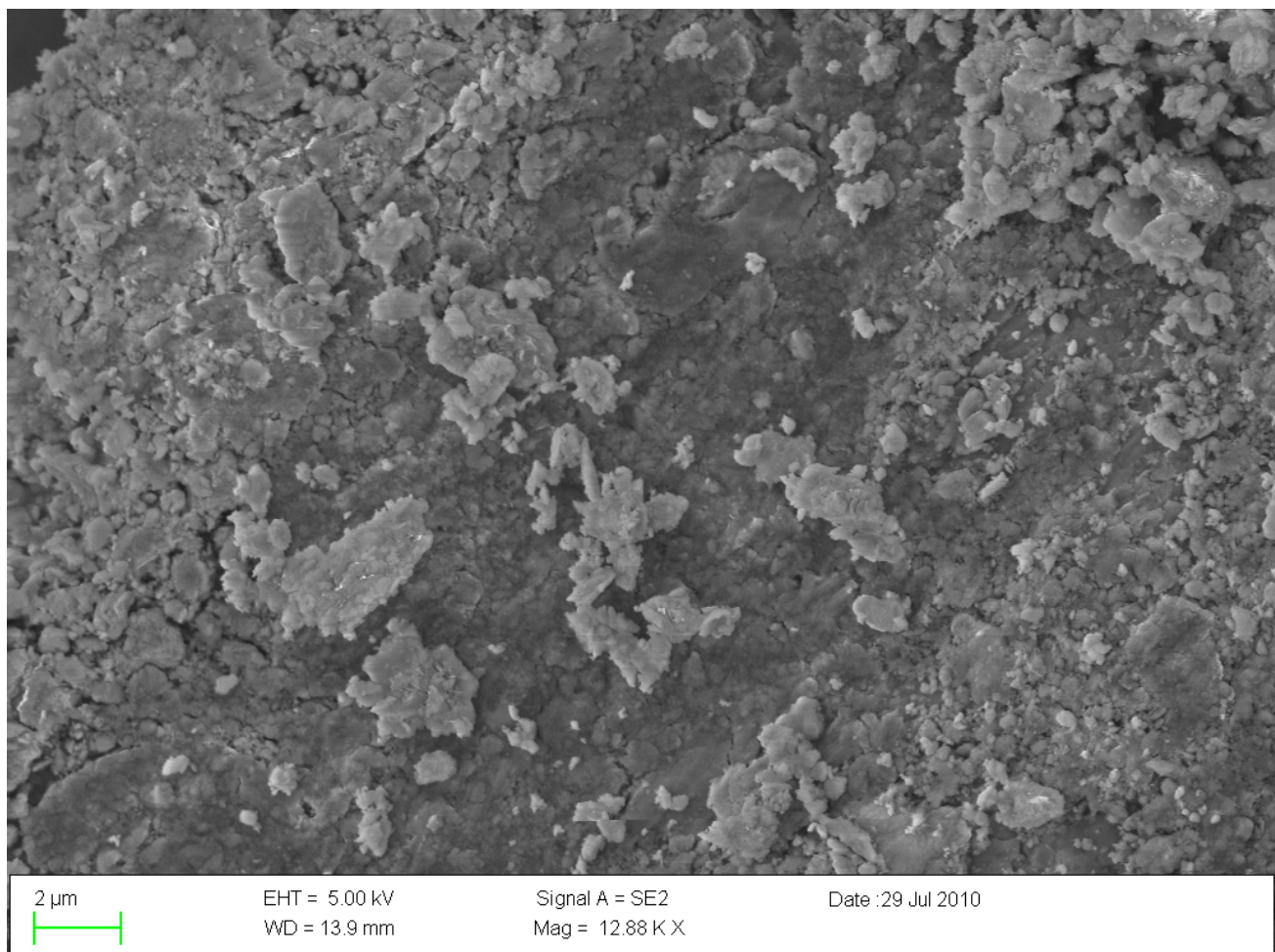


Figure S14. SEM image of as-recovered BnOH-reduced GO showing smaller particles, as well as large area platelets.

TEM Analyses. High resolution transmission electron microscopy (HRTEM) diffraction patterns and images of BnOH-reduced GO were obtained (see Figures S15–S19), and were consistent with the low surface area measured by BET surface analysis and the imagery seen via SEM. The lattice fringes observed in the diffraction pattern (Figure S15) were consistent with a disordered stacking morphology.

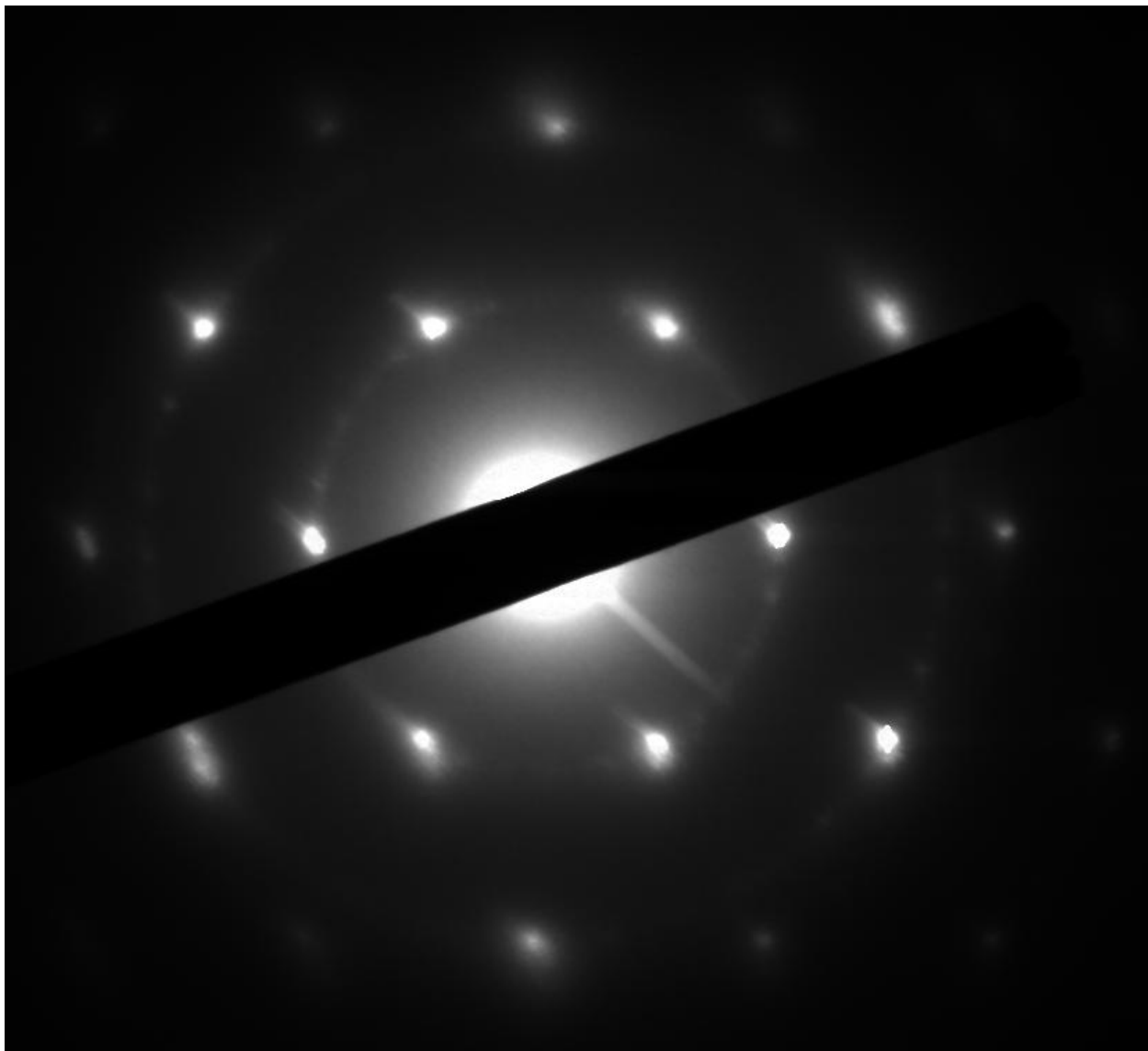


Figure S15. TEM diffraction pattern of as-recovered BnOH-reduced GO showing lattice fringe patterns due to disordering in the stacked structure.

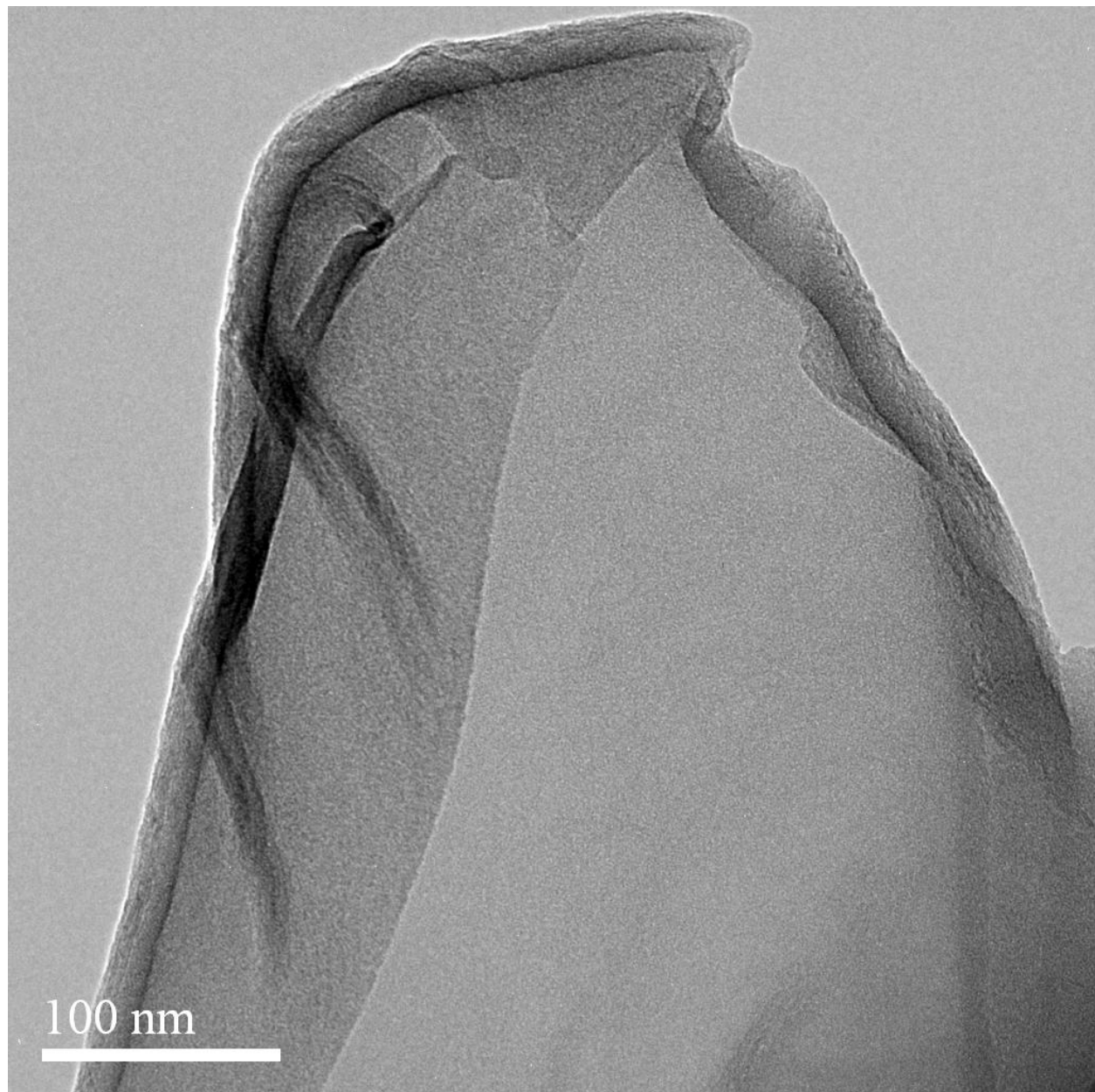


Figure S16. High resolution TEM (HRTEM) image of as-recovered BnOH-reduced GO showing a lamellar morphology.

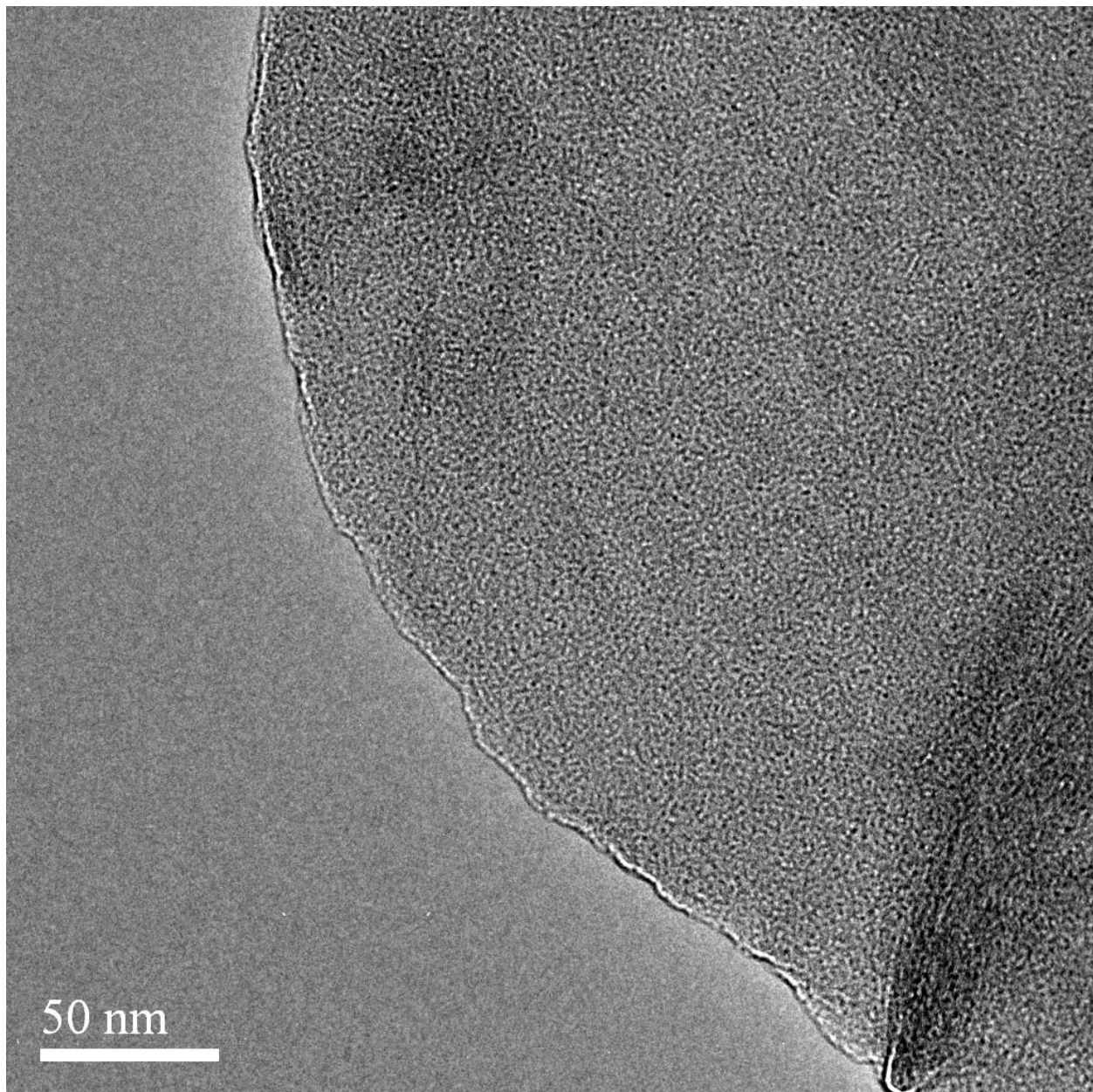


Figure S17. High resolution TEM (HRTEM) image of as-recovered BnOH-reduced GO showing a lamellar morphology.

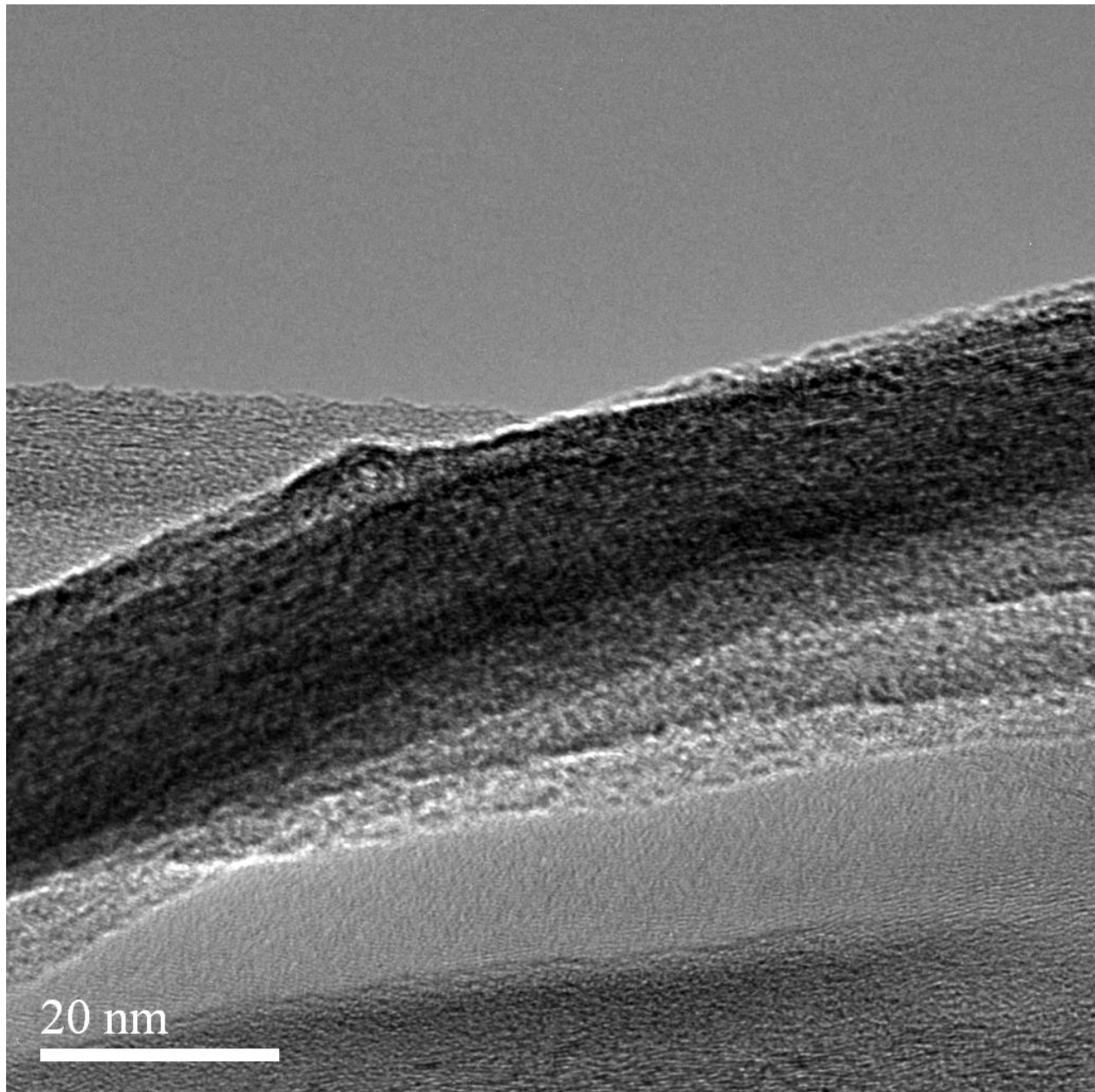


Figure S18. High resolution TEM (HRTEM) image of as-recovered BnOH-reduced GO showing a lamellar morphology.

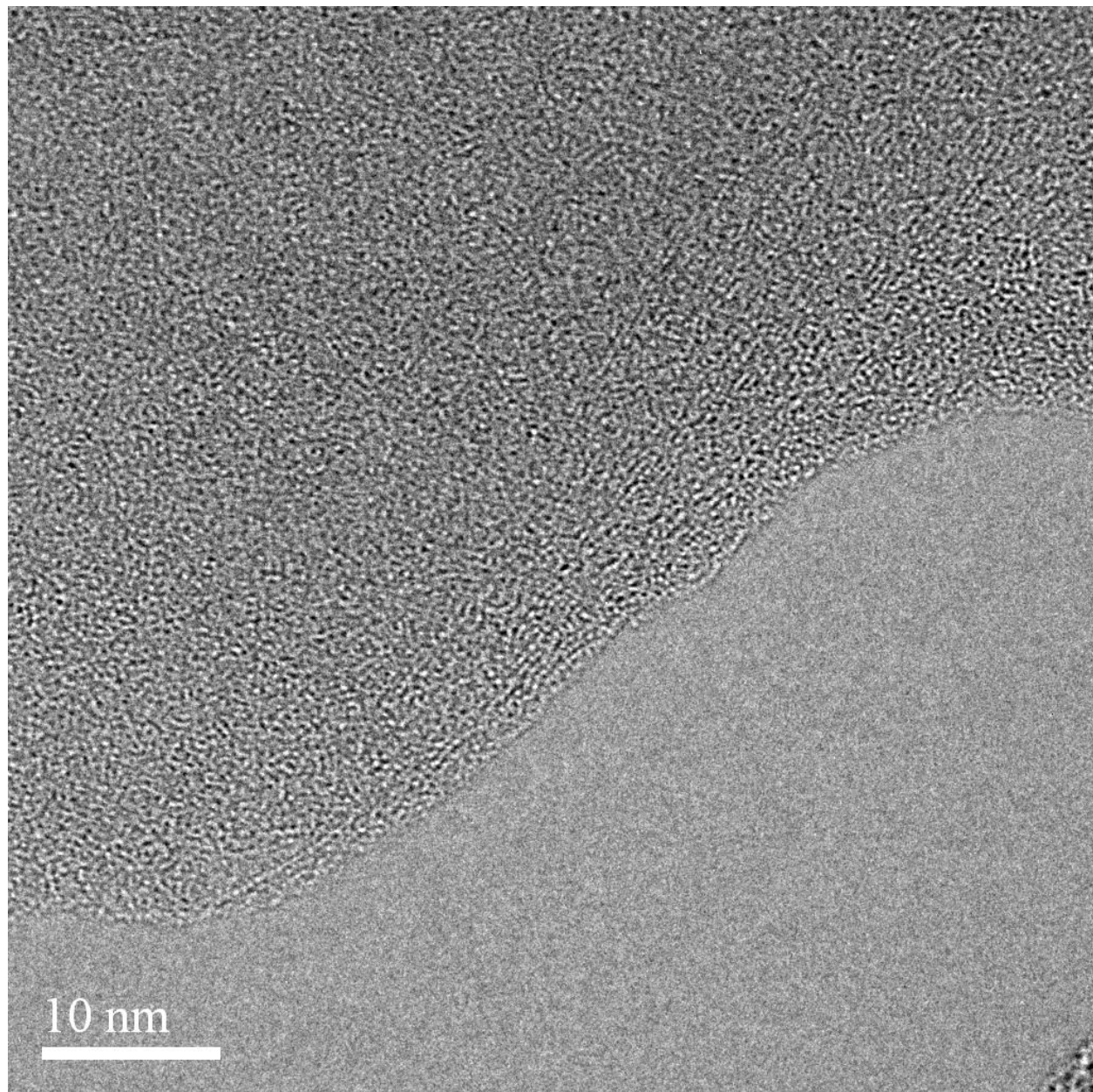


Figure S19. High resolution TEM (HRTEM) image of as-recovered BnOH-reduced GO showing a lamellar morphology.

Ultracapacitor Characterization. Electrodes were fabricated from the iPrOH- and BnOH-reduced carbon materials by mixing 25 mg of the carbon with 2.5 μ L of PTFE (60 wt% dispersion in water). The mixture was ground with a mortar and pestle until a homogeneous, cohesive blend was obtained. The composite was rolled to a thickness of approximately 70 μ m using an aluminum rolling pin. Electrodes that were 1 cm in diameter were cut from the film using a punch. These electrodes were soaked in pairs in 6 M KOH for 12 h, after which time they were assembled into test cells according to the schematic shown in Figure S20 (Celgard[®] 3501 used as the separator and ExopackTM 2.35 mil vinyl [Product #2267] used as the current collector). The performance of the ultracapacitor cells was analyzed using cyclic voltammetry (CV; scan rate: 5–100 mV·s⁻¹), galvanostatic charge/discharge (current: 5–20 mA; Figure S21), and frequency response analysis (FRA) via a Nyquist plot (Figure S22).⁴ The specific capacitance using the CV curves was reported by integrating over the full CV curve to determine the average value.

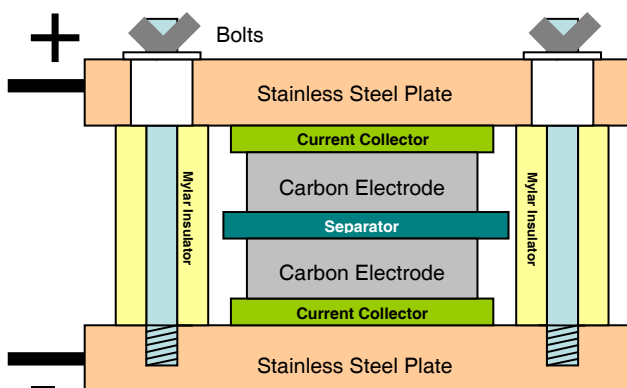


Figure S20. Schematic of a two-electrode test cell assembly.

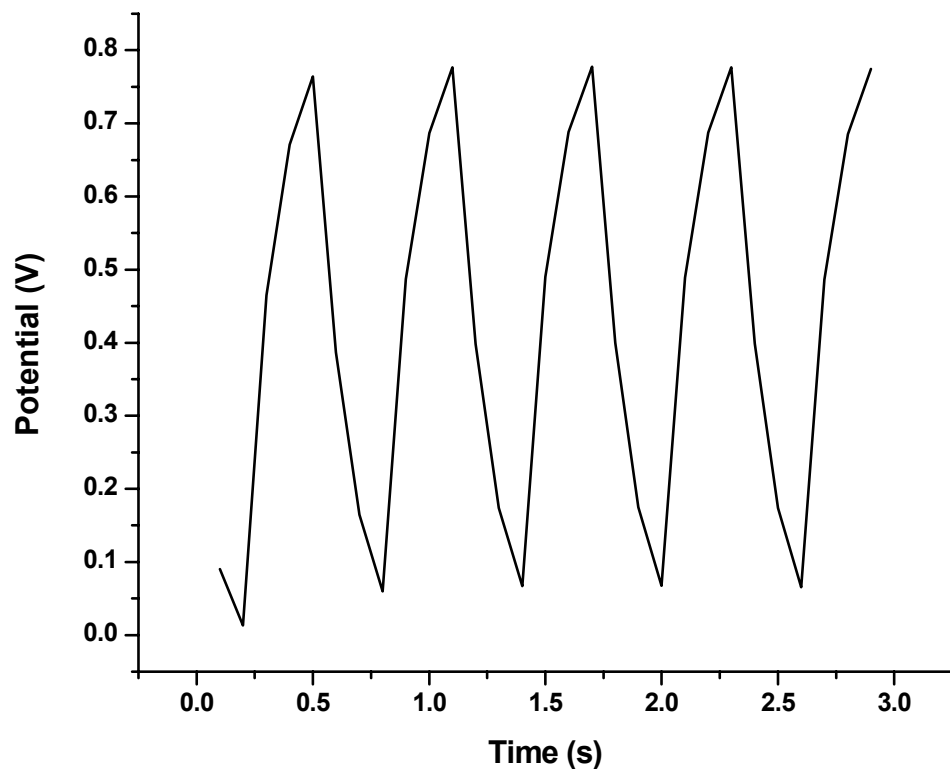


Figure S21. Galvanostatic charge-discharge (applied current: 10 mA) for GO reduced by benzyl alcohol using aqueous KOH as the electrolyte.

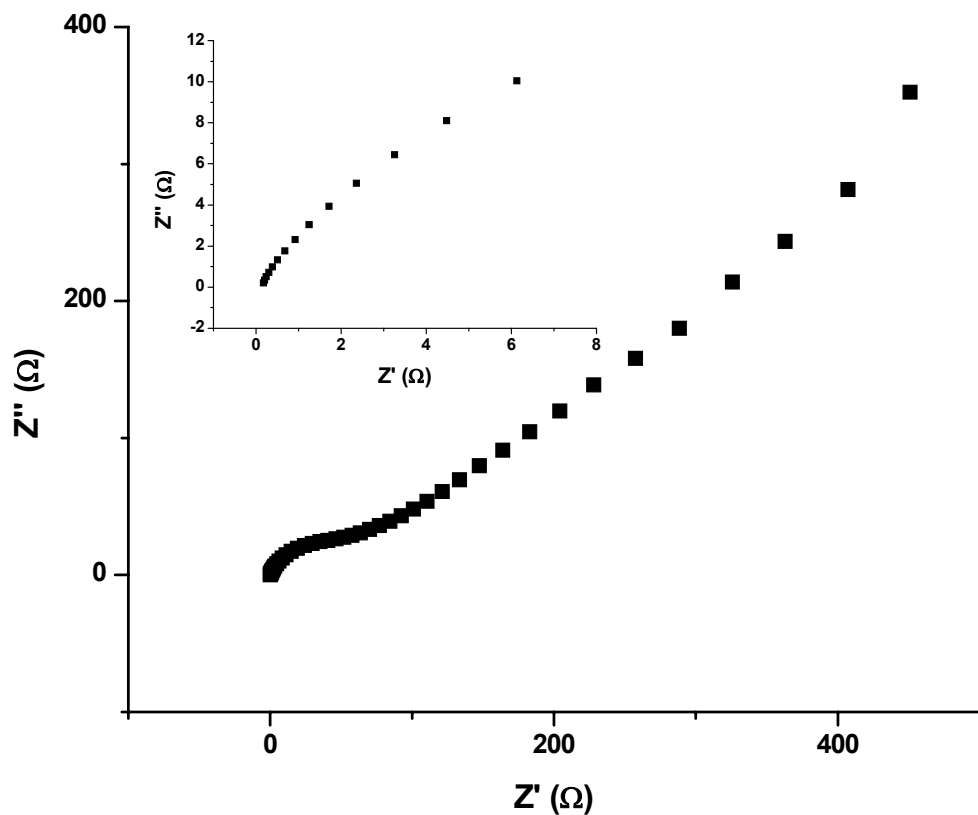


Figure S22. Nyquist plot for GO reduced by benzyl alcohol at a frequency range of 0.02–90,000 Hz (expansion shown in inset).

References

1. (a) Hummers, W. S., Jr.; Offeman, R. E. *J. Am. Chem. Soc.* **1958**, *80*, 1339. (b) Lerf, A.; He, H.; Forster, M.; Klinowski, J. *J. Phys. Chem. B* **1998**, *102*, 4477–4482.
2. Brunauer, S.; Emmett, P. H.; Teller, E.; *J. Am. Chem. Soc.* **1938**, *60*, 309–319.
3. (a) Stankovich, S.; Dikin, D. A.; Piner, R. D.; Kohlhaas, K. A.; Kleinhammes, A.; Jia, Y.; Wu, Y.; Nguyen, S. T.; Ruoff, R. S.; *Carbon*, **2007**, *45*, 1558–1565. (b) Zhu, Y.; Murali, S.; Stoller, M. D.; Velamakanni, A.; Piner, R. D.; Ruoff, R. S.; *Carbon*, **2010**, *48*, 2118–2122.
4. Stoller, M. D.; Park, S.; Zhu, Y.; An, J.; Ruoff, R. S. *Nano Lett.* **2008**, *8*, 3498–3502.